https://doi.org/10.1016/j.jmmm.2021.168130

This is the Pre-Published Version.

Strain dependent structure and anomalous Hall effect in $Pt/Tb_3Fe_5O_{12}/Ga_3Gd_5O_{12}$ heterostructure grown on $Y_3Al_5O_{12}$ substrates

Y.K. Liu[1,2], J.M. Liang[2], H.F. Wong[2], S.M. Ng[2], C.L. Mak[2] and C.W. Leung[2*]

1. College of Electronic Information and Mechatronic Engineering, Zhaoqing University, Zhaoqing Road, Duanzhou District, Zhaoqing 526061, Guangdong, China
2. Department of Applied Physics, The Hong Kong Polytechnic University, Hung Hom, Hong Kong, China

Abstract: We systematically investigate the strain-dependent microstructure and anomalous Hall effect in $Pt/Tb_3Fe_5O_{12}$ (TbIG) grown on (111)-oriented $Y_3Al_5O_{12}$ (YAG) substrates with different thickness of $Ga_3Gd_5O_{12}$ (GGG) buffer layer. Structural measurements indicated that the out-of-plane lattice spacing of TbIG layers firstly increased with the rising thickness of GGG (t_G) and then decreased, which was attributed to the impact of the buffer layer on strain relaxation of the epitaxial films. A variation of compensation temperature was found at t_G about 30 nm. Furthermore, both the anomalous Hall resistance and its sign change temperature increased and then kept constant with increasing t_G. Our results indicated that strain played a key role to tune the physical properties of Pt/TbIG/GGG heterostructures, providing a possible approach to tune the spin-orbital coupling in heavy metal/ferromagnetic insulator system by strain engineering.

Keywords: $Tb_3Fe_5O_{12}$ thin film, Strain effect, Compensation temperature, Anomalous Hall effect

*C.W. Leung, corresponding author

E-mail: dennis.leung@polyu.edu.hk

© 2021. This manuscript version is made available under the CC-BY-NC-ND 4.0 license http://creativecommons.org/licenses/by-nc-nd/4.0/.

Introduction

Recently strain engineering is frequently deployed as an approach to control the properties of complex oxide functional materials [1-5], where the epitaxial strain is strongly coupled with lattice, spin, and orbital of these materials. One can therefore manipulate properties such as charger transfer, spin or orbital reconstruction, interfacial structure transition (such as metal-insulator transition in manganites [2, 6]), structure transition, and giant ferroelectric polarization in $BiFeO_3$ films [3, 7], inducing ferromagnetism in antiferromagnetic $LuMnO_3$ [8] and $LaMnO_3$ films [5], giant magnetoelectric coupling in multiferroic heterostructures [9, 10], and enhancing superconductivity effects[11, 12].

Iron garnets $Re_3Fe_5O_{12}$ (ReIG, Re: rare earth) are one class of the extensively-investigated magnets for ferromagnetic resonance, microwave applications, and spin dynamics studies [13-17]. ReIG has a face-centered cubic lattice structure (space group *Ia*3*d*) [18, 19] with the octahedral and tetrahedral sites occupied by Fe^{3+} ions while Re^{3+} occupy the dodecahedral positions, and there is a strong coupling between lattice and various properties in ReIG [20-24].

Up to now, the majority of reported ReIG epitaxial films used single-crystal $Gd_3Ga_5O_{12}$ (GGG) as substrates [13-17, 22, 25], which limits the study on the strain-dependent physical properties of ReIG materials [26-28]. Apart from GGG, garnets can also be deposited on $Y_3Al_5O_{12}$ (YAG) substrates; the lattice constants (*a*) of GGG and YAG substrates are 12.376 Å and 12.003 Å, respectively, while the lattice constant of some prototypical ReIG are 12.383 Å for YIG [29], 12.324 Å for TmIG [30], and 12.436 Å for TbIG [22]. Recently, studies on YIG films grown on YAG indicated a linear dependence between magnetocrystalline anisotropy and lattice distortion of YIG, which in turn changes the magnetic properties of garnet films and affects the spin-electronic coupling in Pt/YIG

bilayers [21]. Further studies on the strain-dependent spin current behavior in Pt/ReIG heterostructure will provide a better understanding in interfacial coupling between Pt and ReIG, but such studies are lacking.

In this work, we grow high-quality TbIG films on YAG (111) substrates by pulsed laser deposition (PLD). Using GGG as a buffer layer, we control the strain in TbIG and systematically investigated the dependence of the anomalous Hall effect (AHE) in Pt/TbIG/GGG heterostructures on the GGG layer thickness. X-ray diffraction and reciprocal space mappings show an initial increase in the out-of-plane lattice spacing with increasing GGG layer thickness (t_G) but drops with greater t_G, which should be due to the structural distortion for the thin GGG samples and the strain relaxation for thicker GGG samples. Transport measurements show that the temperature at which the sign of the AHE resistance changes is affected by the t_G. Our results suggest that strain engineering is a useful approach to tune the structure of ReIG films and magnetotransport properties of Pt/ReIG bilayers, and can be a possible approach to manipulate the spin-orbit coupling in Pt/ReIG.

Experimental details

TbIG/GGG bilayers were deposited on YAG (111) substrates by PLD at 710˚C and 100 mTorr of oxygen pressure, which were subsequently annealed *in situ* at 710 °C under 10 Torr of oxygen for 10 minutes and then cooled down naturally to room temperature. The thickness of TbIG was fixed at 30 nm, while the thickness of the GGG buffer varied from 0 to 80 nm. The microstructure of the samples was characterized by X-ray diffractometry and reciprocal space mapping measurements (SmartLab, Rigaku Co.) with a Cu Kα_1 radiation (λ = 1.5406 Å). The magnetic properties of the samples were measured by the vibrating sample magnetometer option of a physical property measurement system (PPMS,

Quantum Design). For transport measurements, 5 nm of Pt with Hall bar patterns (channel width: 160 μm, channel length: 500 μm) were deposited on top of TbIG/GGG samples by rf sputtering, in a vacuum chamber of base pressure 1×10^{-7} Torr, using a target power of 60 W.

Results and discussions

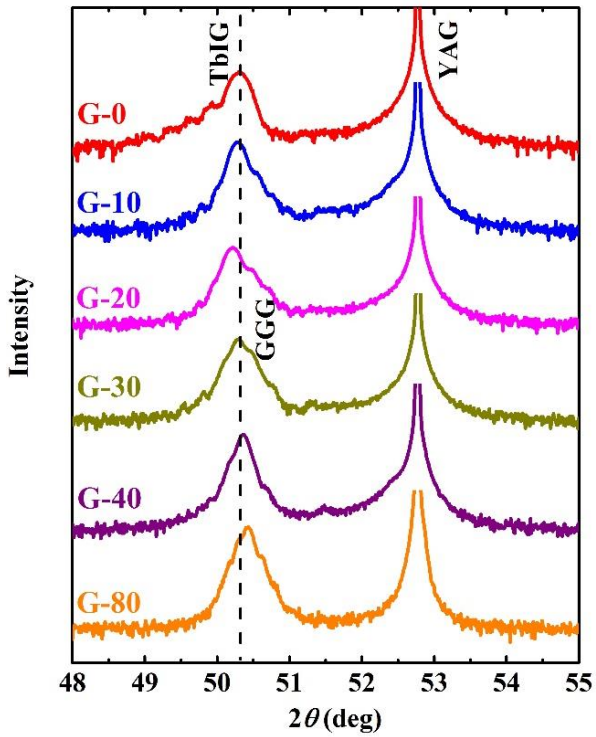

Fig. 1. XRD scans of TbIG/GGG samples around (444) reflections with t_G from 0 to 80 nm. The vertical dash line marks the position of the TbIG film for the G-0 sample (i.e. without GGG buffer).

Table.1 d_{444} value of samples with different GGG thickness

Sample	G-0	G-10	G-20	G-30	G-40	G-80
d_{444} (Å)	1.813	1.814	1.816	1.813	1.810	1.808

Fig. 1 shows the X-ray diffraction (XRD) of TbIG/GGG films around (444) reflections; the d_{444} values of all samples are summarized in Table.1. Without the GGG buffer layer ('G-0' in the figure), one can extract the out-of-plane lattice spacing of d_{444} = 1.813 Å, which is larger than that of bulk value (1.795 Å) due to the compressive in-plane stress from the substrate lattice. By inserting 10 nm thickness of GGG buffer under TbIG ('G-10'), it is found that film peak shifts to a lower angle, indicating the increment of d_{444}. Such a shifting gets more obvious with t_G = 20 nm (G-20). Upon further increasing t_G (G-30, G-40, G-80, respectively), however, the peak position shifts back to a higher angle; in the meantime, the GGG film peak appears and becomes more prominent with increasing t_G. From Fig. 1, one can see the different behavior for the samples with t_G below and above 30 nm.

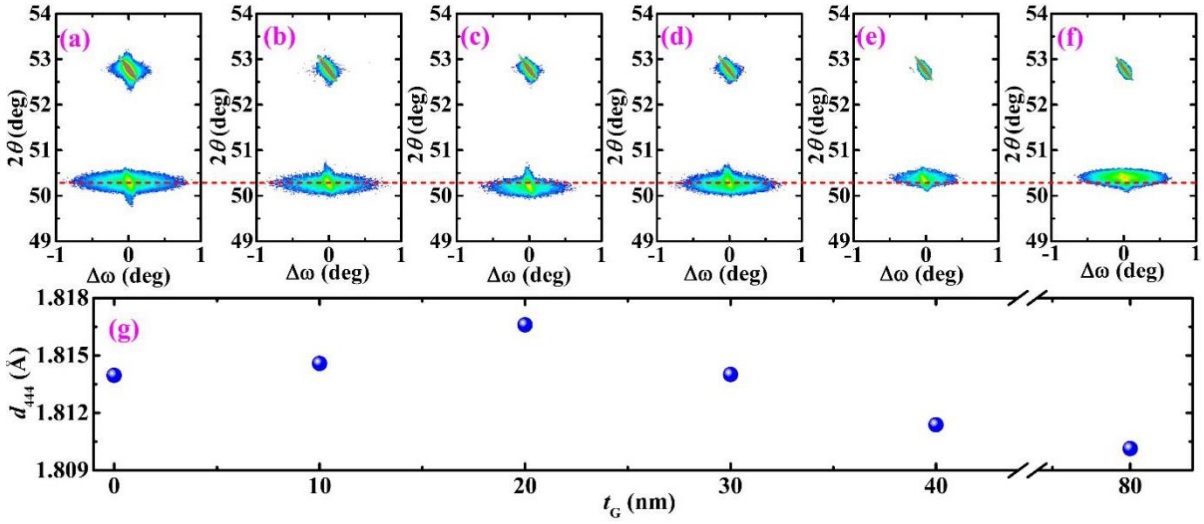

Fig. 2. Reciprocal space maps around (444) reflections of TbIG/GGG samples with different t_G: (a) G-0, (b) G-10, (c) G-20, (d) G-30, (e) G-40, and (f) G-80. The horizontal dashed line marks the position of the TbIG peak of the G-0 sample. (g) shows the t_G dependence of d_{444}- TbIG.

The reciprocal space mappings (RSMs) around (444) reflections of TbIG/GGG bilayers (Fig. 2) clearly show the structure variation with t_G, indicating the coherent growth of the films on YAG substrates. As a reference check, the measured lattice spacing for the YAG substrate is d_{444}=1.7335 Å, corresponding to the cubic lattice parameter a_s = 12.010 Å, in good agreement with the theoretical value 12.003 Å. As for the G-0 sample (Fig. 2(a)), one can get d_{444} = 1.814 Å for TbIG, which is close to that obtained from XRD (Table1). Besides, with increasing t_G the positions of film spots firstly shift to lower angles (Figs. 2(b)-(d)) and then back to high angles for t_G > 30 nm (Figs. 2(e)-(f)). Fig. 2(g) shows the t_G-dependence of the out-of-plane lattice spacing d_{444}, which indicates a nonmonotonic dependence on the thickness of the GGG layer.

Generally, garnets crystalize in the cubic structure, and the lattice parameter of GGG (12.376 Å) is between YAG (12.003 Å) and TbIG (12.436 Å). In principle, the compressive strain for TbIG grown on YAG (~3.48%) is much larger than that of TbIG on GGG (~0.48%), and the insertion of GGG buffer between TbIG and YAG should relax TbIG's in-plane compressive strain and reduce the out-of-plane lattice spacing, as compared with direct deposition of TbIG on YAG. However, our data for TbIG/GGG samples indicated that when t_G is below 30 nm (Figs. 1 & 2) there is a gradual increase of lattice strain in TbIG.

The variation of measured d_{444} value with t_G can be attributed to the impact of GGG buffer on the conformal growth of overlying TbIG. The strain of epitaxial films is highly sensitive to film thickness, and strain relaxation takes place as the thickness goes beyond certain critical values (t_c) which depends on the lattice mismatch between materials [31]. When the thickness is less than t_c the film is fully strained, and an in-plane compression would increase the out-of-plane lattice parameter. Beyond t_c, strain relaxation takes place and subsequent film growth is

not conforming to the substrate, leading to the drop of the lattice parameter. Similar behavior has been observed in BIG ($Bi_3Fe_5O_{12}$) films grown on GGG(001) substrate [32].

We can understand our results as follows. For the G-0 sample, due to the large mismatch between TbIG and YAG, strain relaxation could occur. The GGG layer (with lattice parameter in between TbIG and YAG) would act as a buffer, hence suppressing the relaxation in TbIG and the corresponding d_{444} value, therefore, increase with t_G. With larger t_G strain relaxation eventually takes place in the bilayer due to the substantial thickness, which is manifested as the decreasing d_{444} value with large t_G. The observation also finds support from the full width at half maximum (FWHM) of the rocking curves around (444) reflection of samples with different t_G (Fig. S1, Supplementary Information). The FWHM of the rocking curves is a direct measurement of the mosaic spread of lattices in the samples, thus serving as an indicator for relaxation events. The drop in FHMW with small t_G (Fig. S1) coincides with the rise of d_{444}; beyond t_G = 20 nm a gradual increase in FWHM is observed, alongside a decrease of d_{444} value. On the other hand, one should be cautious about the above interpretation, as the increasing contribution towards the XRD profile by thicker GGG can also induce an apparent shift of the 2θ to higher values, leading to an apparent decrease of the d_{444}. Due to the small lattice mismatch between TbIG and GGG, it is difficult to differentiate the TbIG and GGG layers from our XRD profiles.

Cross-sectional TEM imaging was used to confirm the epitaxial growth, and the result of the G-20 sample is shown in Fig. 3(a). Since the lattice parameters of TbIG and GGG are very close, no obvious lattice mismatch is observed at the interface. The measured thickness of the TbIG and GGG layers (29.1±0.6 nm and 18.7±0.6 nm respectively) are close to the designed values. Cross-sectional

electron diffraction spectroscopy (EDX) mapping across the sample thickness (Fig. 3(b)) for Tb, Gd, and Al (Figs. 3(c)-(e)) demonstrates clear separation between the layers with minimal interlayer diffusion.

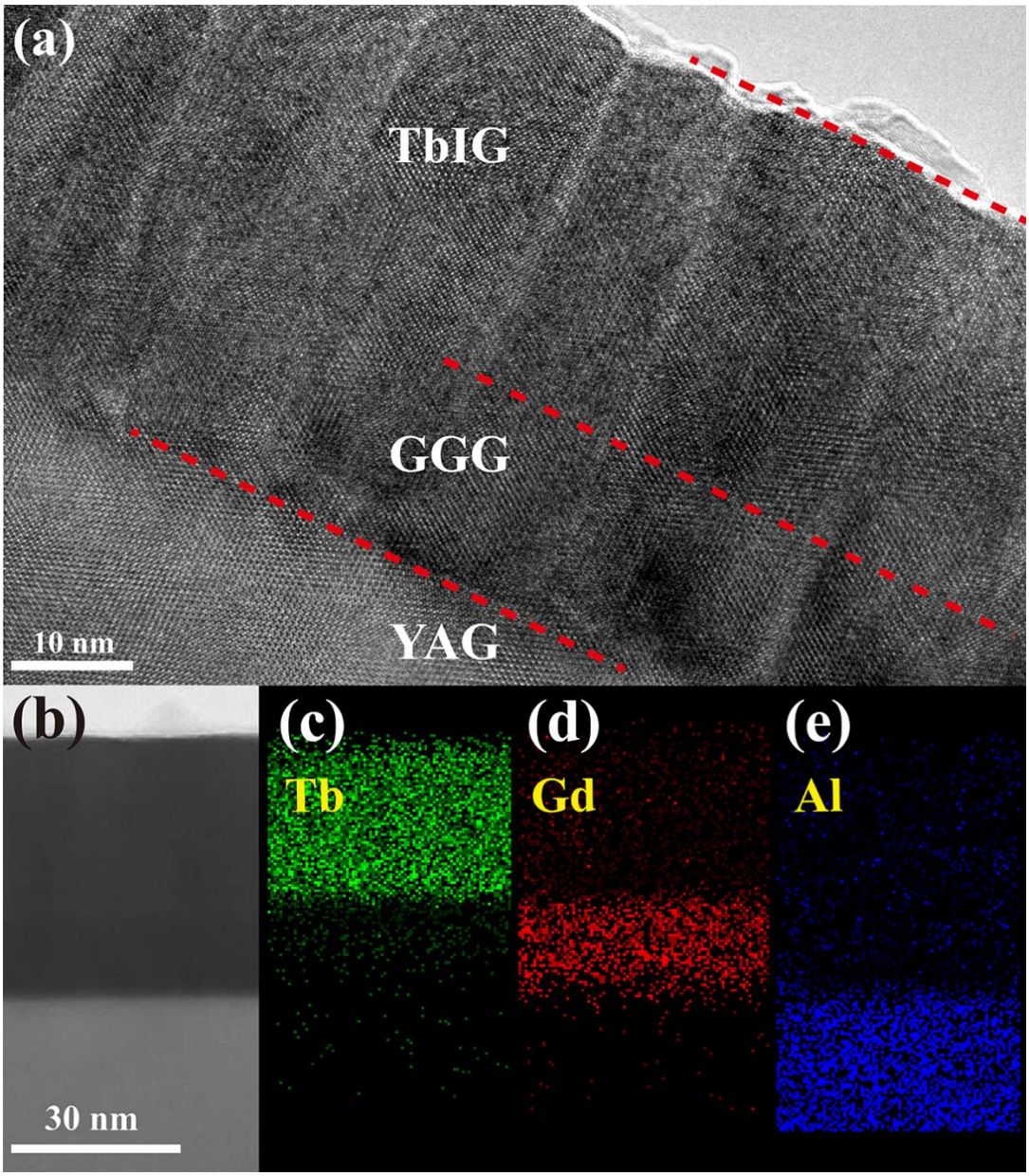

Fig. 3. (a) High-resolution cross-sectional TEM of G-20 sample. (b) to (e) shows the cross-sectional EDX analysis, including the area analyzed (b) and the results for Tb (c), Gd (d), and Al (e), which are unique species in the corresponding layers.

Fig. 4 shows the temperature dependence of magnetization (M-T) of the TbIG/GGG bilayer samples, as measured at a magnetic field of 1000 Oe by warming from 10 K to 400 K. One can find the compensation point (T_{comp}, where the saturation magnetization momentarily vanishes) of the G-0 sample is near 180K, which is smaller than bulk TbIG (~240 K) or TbIG films grown on GGG substrates (~220 K) [22, 33]. The suppressed T_{comp} for TbIG/YAG sample could be attributed to the strain effect as discussed above. With increasing thickness of the GGG buffer, T_{comp} increases up to near 220 K for the G-80 sample, approaching that of TbIG on GGG substrates. The estimation of T_{comp} using the M-T curve is however qualitative, due to the strong magnetization contribution from the GGG buffer layer that is comparable with the TbIG film, especially around T_{comp} and for samples with large t_G.

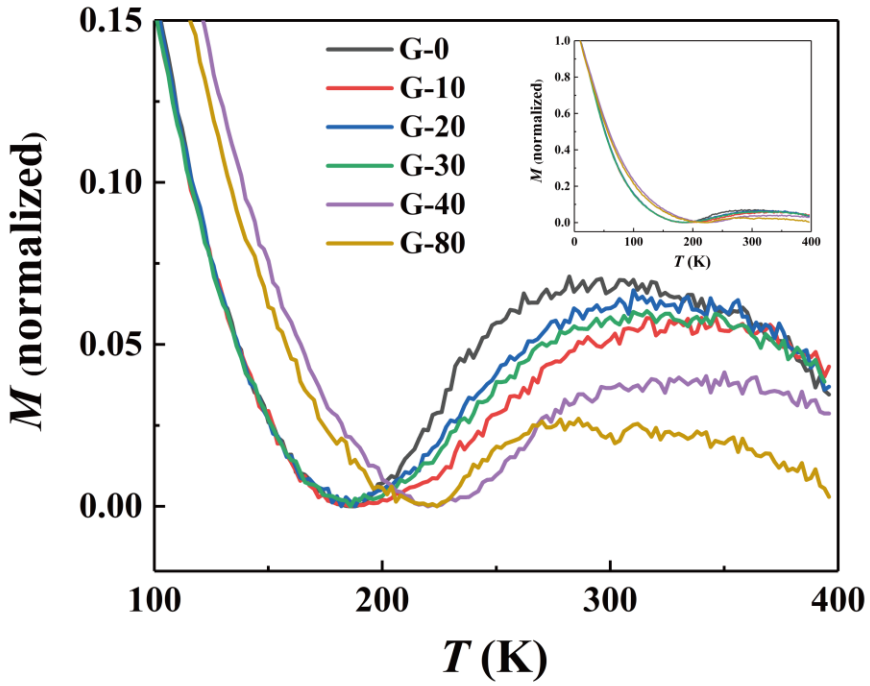

Fig. 4. The M-T curves of TbIG/GGG samples from 100 K to 400 K. The inset shows the M-T curves from 10 K to 400 K.

For transport measurements, TbIG/GGG samples were coated with Pt electrode as described previously, and we refer to such Pt-coated samples by the same terminology (e.g. G-20 sample refer to Pt-coated TbIG with 20 nm GGG buffer) in the following discussions. Results of the transport measurement are illustrated in Fig. 5. In Fig. 5(a) the geometry of measurement is shown as the inset, where the current is applied along the *x*-axis and φ denotes the angle between the applied magnetic field (H) and the *z*-axis in the *y*-*z* plane. The temperature-dependent longitudinal resistance (R_{xx}) of the G-0 sample is shown in Fig. 5(a), with the gradually decreasing R_{xx} upon reducing temperature confirming the metallic behavior of the Pt layer. Similar to cases reported in other Pt/ReIG heterostructures [22, 34], a resistance minimum of around 20 K is observed, which may be resulted from the weak localization of electrons [34].

Fig. 5(b) exhibits the angular dependence of magnetoresistance (ΔR_{xx}) in G-0 sample at 300 K and 10 K, with H = 9 T. Here, ΔR_{xx} is defined as $\Delta R_{xx} = R_{xx}(\varphi) - R_{xx}(90°)$, where $R_{xx}(\varphi)$ and $R_{xx}(90°)$ are the resistances at angle φ and 90°. The amplitude of ΔR_{xx} shows a small increase with temperature decreasing from 300 K to 10 K, possibly due to the slightly enhanced TbIG magnetic moment with decreasing temperature.

As for the transverse resistance R_{xy} (Fig. 5(c)), it shows a different angular dependence compared to that of ΔR_{xx}: not only is the amplitude of R_{xy} decrease more dramatically with increasing temperature but also a sign reversal is observed. Here, R_{xy} should contain two contributions: the ordinary Hall effect (OHE) contribution (with a linear dependence on the applied magnetic field) and an AHE part which is proportional to the magnetization of FM and is closely related to the spin-orbital interaction. Importantly, when the magnetic field is applied normal to the film (φ = 0°), the value of R_{xy} will reach maximum, indicating a maximum

AHE can be found at $\varphi = 0°$. That is, with increasing temperature from 10 K to 300 K, the sign of AHE has been changed according to Fig. 5(c).

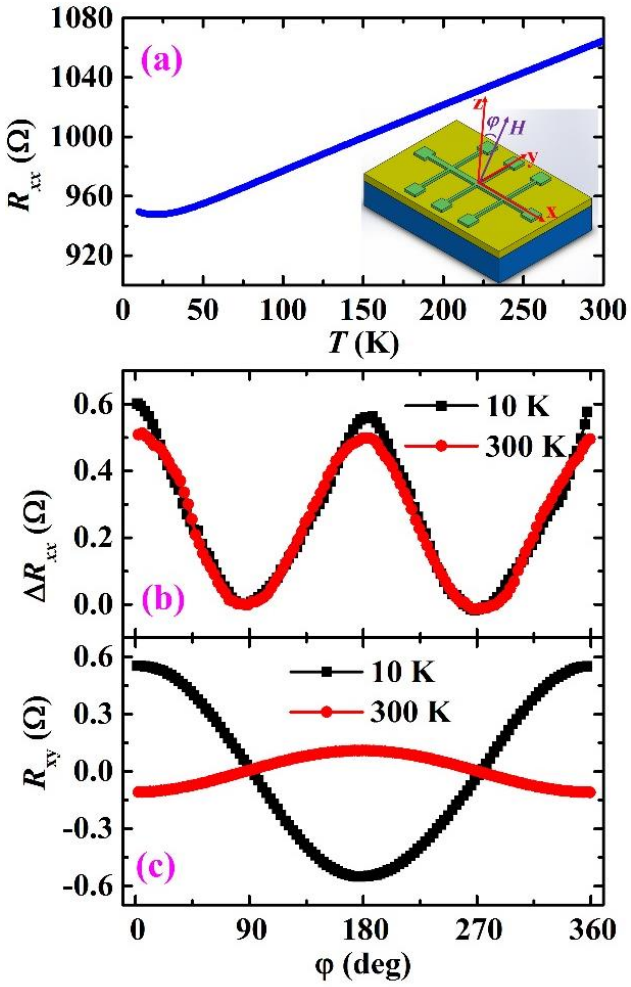

Fig. 5. (a) Temperature dependence of R_{xx} in G-0 sample with Pt electrodes. Inset shows the schematic for the measurements where the current is applied along the *x*-axis and φ denotes the angle between the applied magnetic field *H* and the *z* axis. (b) and (c) show the angular dependent ΔR_{xx} and R_{xy} at 9 T for G-0 and two different temperatures of 10 K and 300 K.

To observe the AHE sign change, we measured the anomalous Hall resistance R_{Hall} vs. *H* (R_{Hall}-*H*, where $\varphi = 0°$) at different temperatures for various samples (Fig. 6), where the linear contribution at high magnetic fields have been subtracted. At 10 K, the value of R_{Hall} at 9 T ($R_{\text{Hall}}^{9\text{T}}$) is about 0.35 Ω for G-0 sample (Fig. 6(a)),

and it reduces with increasing temperature. Around 70 K, the sign of R_{Hall} changes, which is similar to that observed in Pt/YIG structures [35-37]. Our previous study has found a reversal of the AHE sign occurred twice in Pt/TbIG grown on GGG substrates [22]: while the reversal at 50 K in the previous report is similar to our present data, there is another sign reversal event around the compensation point of TbIG (~ 220 K) [30]. The appearance of compensation point in TbIG is due to the antiferromagnetic coupling of Tb^{3+} and Fe^{3+} sublattice moments, and at some temperatures, they become identical to each other and results in a net-zero moment [30]. As the anisotropy axis of TbIG/GGG on YAG(111) is in-plane regardless of t_G value, square-shaped AHE resistance loop as well as its sign change near the T_{comp} cannot be observed in our measurements [22].

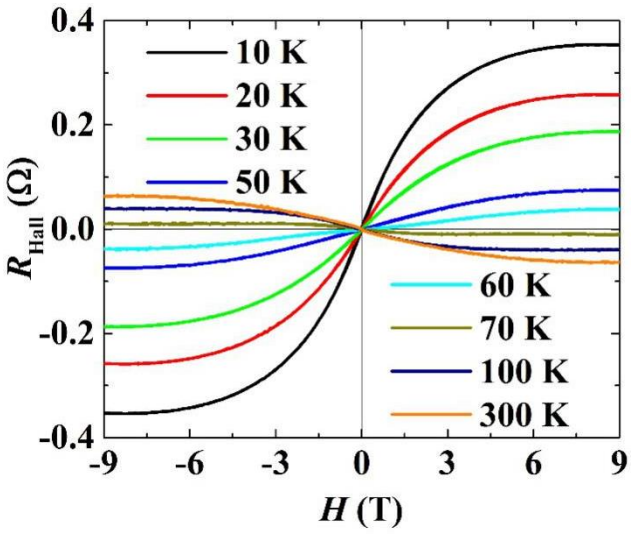

Fig. 6. Magnetic field dependence of AHE of G-0 sample at different temperatures.

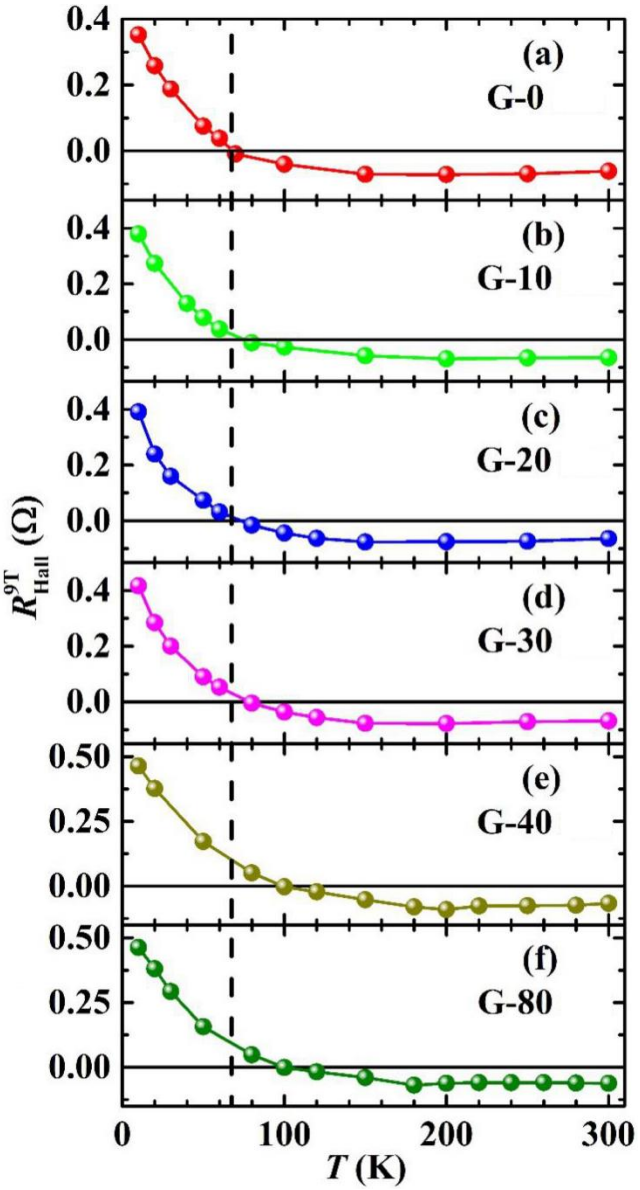

Fig. 7. Temperature dependence of $R_{\mathrm{Hall}}^{9\mathrm{T}}$ with different GGG buffer layer thicknesses: (a) G-0, (b) G-10: 10nm, (c) G-20: 20 nm, (d) G-30: 30nm, (e) G-40: 40 nm, (f) G-80: 80 nm. The vertical dashed line indicates the AHE sign change temperature of the G-0 sample.

Here, we systematically study the t_{G} dependence of $R_{\mathrm{Hall}}^{9\mathrm{T}}$. From Fig. 7, one can find that all the samples show a drop of $R_{\mathrm{Hall}}^{9\mathrm{T}}$ with increasing temperatures, and sign reversal of AHE has taken place around 100 K or below. Comparing the amplitude of $R_{\mathrm{Hall}}^{9\mathrm{T}}$ at 10 K for different samples, it was found to be enhanced with increasing t_{G} up to 30 nm as shown in Figs.7(b)-(d). With further increasing t_{G} to

40 nm and above, $R_{\mathrm{Hall}}^{9\mathrm{T}}$ is saturated at about 0.46 Ω (Figs.7(e) & (f)). As for the T_{sign}, it drifts slowly to higher temperatures with increasing t_{G}.

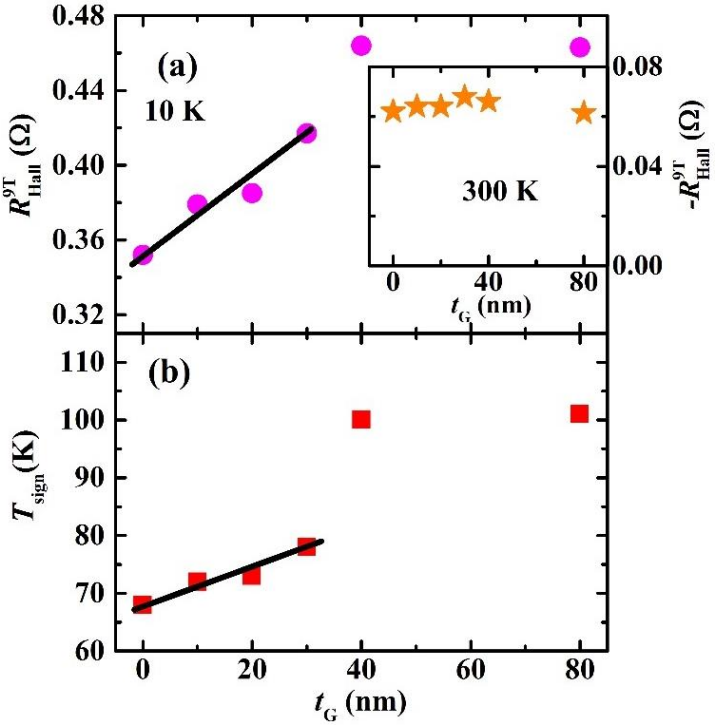

Fig. 8. t_{G} dependence of $R_{\mathrm{Hall}}^{9\mathrm{T}}$ (b) at 10 K and T_{sign} (b). Inset of (a) shows the t_{G} dependent $R_{\mathrm{Hall}}^{9\mathrm{T}}$ at 300 K. The black lines indicate the linear dependence for $t_{\mathrm{G}} \leq 30$ nm.

The t_{G} dependences of $R_{\mathrm{Hall}}^{9\mathrm{T}}$ and T_{sign} are extracted and the results are as shown in Fig. 8. As for the $R_{\mathrm{Hall}}^{9\mathrm{T}}$ (Fig.9a), it shows an almost linear dependence for $t_{\mathrm{G}} \leq 30$ nm and then saturates above 40 nm. As for at 300 K (inset of Fig. 8(a)), $R_{\mathrm{Hall}}^{9\mathrm{T}}$ demonstrates little variation with t_{G} and is kept around 0.06 Ω, which is much smaller than that at 10 K. For T_{sign} (Fig. 8(b)), it shows a linear increase with rising t_{G} below 30 nm and reaches up to 100 K at 40 nm, beyond which it shows little variation. Thus, with rising t_G an enhanced AHE resistance in TbIG/GGG at the low-temperature region is obtained, alongside an increment of T_{sign}.

Conclusion

In summary, we investigated the impact of the GGG buffer layer on the strain of TbIG films and the anomalous Hall effect in Pt/TbIG epitaxially grown on YAG(111) substrates. Around a critical thickness of 20 nm, the out-of-plane lattice parameters of the TbIG/GGG samples first increase and then decrease, respectively. This is suggested to arise from the effect of the GGG insert on the strain relaxation of the TbIG/GGG bilayers. In addition, the anomalous Hall resistance and the sign reversal temperature increase with rising GGG buffer layer and gradually saturates. The GGG thickness-dependences of various properties indicate that the strain plays a key role, and our results suggest a possible approach way to manipulate the spin transport and spin-orbital coupling in the heavy metal/ferromagnetic insulator system.

Acknowledgment

Financial supports from RGC, HKSAR (PolyU 15302320), and PolyU (G-ZVGH, G-ZVQH) are acknowledged.

References:

[1] C. Becher, L. Maurel, U. Aschauer, M. Lilienblum, C. Magén, D. Meier, E. Langenberg, M. Trassin, J. Blasco, I. P. Krug, P. A. Algarabel, N. A. Spaldin, J. A. Pardo and M. Fiebig, Strain-induced coupling of electrical polarization and structural defects in $SrMnO_3$ films, Nat. Nanotechnol, **10** (2015) 661-665.

[2] K. H. Ahn, T. Lookman, and A. R. Bishop, Strain-induced metal–insulator phase coexistence in perovskite manganites, Nature **428** (2004) 401-404.

[3] R. J. Zeches, M. D. Rossell, J. X. Zhang, A. J. Hatt, Q. He, C. H. Yang, A. Kumar, C. H. Wang, A. Melville, C. Adamo, G. Sheng, Y. H. Chu, J. F. Ihlefeld, R. Erni, C. Ederer, V. Gopalan, L. Q. Chen, D. G. Schlom, N. A. Spaldin, L. W. Martin, R. Ramesh, A Strain-Driven Morphotropic Phase Boundary in $BiFeO_3$, Science **326** (2009) 977-980.

[4] X. Z. Lu and J. M. Rondinelli, Epitaxial-strain-induced polar-to-nonpolar transitions in layered oxides, Nat. Mater, **15** (2016) 951-955.

[5] Y. K. Liu, H. F. Wong, K. K. Lam, C. L. Mak, and C. W. Leung, Tuning ferromagnetic properties of $LaMnO_3$ films by oxygen vacancies and strain, J. Magn. Magn. Mater, **481** (2019) 85-92 .

[6] Y. K. Liu, Y. W. Yin, and X. G. Li, Colossal magnetoresistance in manganites and related prototype devices, Chin. Phys. B, **22** (2013) 087502.

[7] J. X. Zhang, Q. He, M. Trassin, W. Luo, D. Yi, M. D. Rossell, P. Yu, L. You, C. H. Wang, C. Y. Kuo, J. T. Heron, Z. Hu, R. J. Zeches, H. J. Lin, A. Tanaka, C. T. Chen, L. H. Tjeng, Y. H. Chu, and R. Ramesh, Microscopic Origin of the Giant Ferroelectric Polarization in Tetragonal-like $BiFeO_3$, Phys. Rev. Lett, **107** (2011) 147602.

[8] J. S. White, M. Bator, Y. Hu, H. Luetkens, J. Stahn, S. Capelli, S. Das, M. Döbeli, Th. Lippert, V. K. Malik, J. Martynczuk, A. Wokaun, M. Kenzelmann, Ch. Niedermayer, and C. W. Schneider, Strain-Induced Ferromagnetism in Antiferromagnetic $LuMnO_3$ Thin Films, Phys Rev Lett **111** (2013) 037201 .

[9] S. Zhang, Y. G. Zhao, P. S. Li, J. J. Yang, S. Rizwan, J. X. Zhang, J. Seidel, T. L. Qu, Y. J. Yang, Z. L. Luo, Q. He, T. Zou, Q. P. Chen, J. W. Wang, L. F. Yang, Y. Sun, Y. Z. Wu, X. Xiao, X. F. Jin, J. Huang, C. Gao, X. F. Han, and R. Ramesh, Electric-Field Control of Nonvolatile Magnetization in $Co_{40}Fe_{40}B_{20}/Pb(Mg_{1/3}Nb_{2/3})_{0.7}Ti_{0.3}O_3$ Structure at Room Temperature, Phys. Rev. Lett. **108** (2012) 137203.

[10] N. Lei, S. Park, P. Lecoeur, D. Ravelosona, C. Chappert, O. Stelmakhovych, and V. Holý, Magnetization reversal assisted by the inverse piezoelectric effect in Co-Fe-B/ferroelectric multilayers, Phys. Rev. B **84** (2011) 012404.

[11] J. F. Ge, Z. L. Liu, C. Liu, C. L. Gao, D. Qian, Q. K. Xue, Y. Liu, and J. F. Jia, Superconductivity above 100 K in single-layer FeSe films on doped $SrTiO_3$, Nat. Mater. **14** (2014) 285-289.

[12] I. Bozovic, G. Logvenov, I. Belca, B. Narimbetov, and I. Sveklo, Epitaxial Strain and Superconductivity in $La_{2-x}Sr_xCuO_4$ Thin Films, Phys Rev Lett **89** (2002) 107001.

[13] Y. Kajiwara, K. Harii, S. Takahashi, J. Ohe, K. Uchida, M. Mizuguchi, H. Umezawa, H. Kawai, K. Ando, K. Takanashi, S. Maekawa & E. Saitoh, Transmission of electrical signals by spin-wave interconversion in a magnetic insulator, Nature **464** (2010) 262-266.

[14] H. Nakayama, M. Althammer, Y. T. Chen, K. Uchida, Y. Kajiwara, D. Kikuchi, T. Ohtani, S. Geprägs, M. Opel, S. Takahashi, R. Gross, G. E. W. Bauer, S. T. B. Goennenwein, and E. Saitoh, Spin Hall Magnetoresistance Induced by a Nonequilibrium Proximity Effect, Phys. Rev. Lett. **110** (2013) 206601.

[15] W. Lin and C. L. Chien, Electrical Detection of Spin Backflow from an Antiferromagnetic Insulator/$Y_3Fe_5O_{12}$ Interface, Phys.Rev. Lett. **118** (2017) 067202.

[16] C. O. Avci, A. Quindeau, C. F. Pai, M. Mann, L. Caretta, Astera S. Tang, M. C. Onbasli, C. A. Ross, and G. S. D. Beach, Current-induced switching in a magnetic insulator, Nat. Mater. **16** (2017) 309-314.
[17] J. Cramer, E. J. Guo, S. Geprägs, A. Kehlberger, Y. P. Ivanov, K. Ganzhorn, F. D. Coletta, M. Althammer, H. Huebl, R. Gross, J. Kosel, M. Kläui, and S. T. B. Goennenwein, Magnon Mode Selective Spin Transport in Compensated Ferrimagnets, Nano letters **17** (2017) 3334-3340.
[18] S. Geller and M. A. Gilleo, The crystal structure and ferrimagnetism of yttrium-iron garnet, $Y_3Fe_2(FeO_4)_3$, J. Phys. Chem. Solids **3** (1957) 30-36.
[19] F. Sayetat, Huge magnetostriction in $Tb_3Fe_5O_{12}$, $Dy_3Fe_5O_{12}$, $Ho_3Fe_5O_{12}$, $Er_3Fe_5O_{12}$ garnets, J. Magn. Magn. Mater, **58** (1986) 334-346.
[20] J. L. Wu, G. Gundiah, and A. K. Cheetham, Structure–property correlations in Ce-doped garnet phosphors for use in solid state lighting, Chem. Phys. Lett. **441** (2007) 250-254.
[21] C. S. Wolfe, V. P. Bhallamudi, H. L. Wang, C. H. Du, S. Manuilov, R. M. Teeling-Smith, A. J. Berger, R. Adur, F. Y. Yang, and P. C. Hammel, Off-resonant manipulation of spins in diamond via precessing magnetization of a proximal ferromagnet, Phys. Rev. B **89** (2014) 180406.
[22] Y. K. Liu, H. F. Wong, K. K. Lam, C. L. Mak, and C. W. Leung, Anomalous Hall effect in $Pt/Tb_3Fe_5O_{12}$ heterostructure: Effect of compensation point, J. Magn. Magn. Mater. **468** (2018) 235-240
[23] E. R. Rosenberg, L. Beran, C. O. Avci, C. Zeledon, B. Q. Song, C. Gonzalez-Fuentes, J. Mendil, P. Gambardella, M. Veis, C. Garcia, G. S. D. Beach, and C. A. Ross, Magnetism and spin transport in rare-earth-rich epitaxial terbium and europium iron garnet films, Phys. Rev. Mater. **2** (2018) 094405
[24] V. H. Ortiz, M. Aldosary, J. X. Li, Y. D. Xu, M. I. Lohmann, P. Sellappan, Y. Kodera, J. E. Garay, and J. Shi, Systematic control of strain-induced perpendicular magnetic anisotropy in epitaxial europium and terbium iron garnet thin films, APL Mater. **6** (2018) 121113
[25] A. Quindeau, C. O. Avci, W. Q. Liu, C. L. Sun, M. Mann, A. S. Tang, M. C. Onbasli, D. Bono, P. M. Voyles, Y. B. Xu, J. Robinson, G. S. D. Beach, C. A. Ross, $Tm_3Fe_5O_{12}$/Pt Heterostructures with Perpendicular Magnetic Anisotropy for Spintronic Applications, Adv. Electron. Mater. **3** (2017) 1600376.
[26] H. Yamahara, M. Mikami, M. Seki, and H. Tabata, Epitaxial strain-induced magnetic anisotropy in $Sm_3Fe_5O_{12}$ thin films grown by pulsed laser deposition, J. Magn. Magn. Mater. **323** (2011) 3143-3146.
[27] M. Kubota, A. Tsukazaki, F. Kagawa, K. Shibuya, Y. Tokunaga, M. Kawasaki, and Y. Tokura, Stress-Induced Perpendicular Magnetization in Epitaxial Iron Garnet Thin Films, Appl. Phys. Express **5** (2012) 103002.
[28] V. H. Ortiz, M. Aldosary, J. Li, Y. Xu, M. I. Lohmann, P. Sellappan, Y. Kodera, J. E. Garay, and J. Shi, Systematic control of strain-induced perpendicular magnetic anisotropy in epitaxial europium and terbium iron garnet thin films, APL Mater. **6** (2018) 121113.
[29] C. Tang, M. Aldosary, Z. Jiang, H. Chang, B. Madon, K. Chan, M. Wu, J. E. Garay, and J. Shi, Exquisite growth control and magnetic properties of yttrium iron garnet thin films, Appl. Phys. Lett. **108** (2016) 102403.
[30] C. Tang, P. Sellappan, Y. Liu, Y. Xu, J. E. Garay, and J. Shi, Anomalous Hall hysteresis in $Tm_3Fe_5O_{12}$/Pt with strain-induced perpendicular magnetic anisotropy, Phys. Rev. B **94** (2016) 140403.
[31] E. Popova, M. Deb, L. Bocher, A. Gloter, O. Stéphan, B. Warot-Fonrose, B. Berini, Y. Dumont, and N. Keller, Interplay between epitaxial strain and low dimensionality effects in a ferrimagnetic oxide, J. Appl. Phys. **121** (2017) 115304.
[32] E. Popova, A. Gloter, M. Deb, B. Warot-Fonrose, H. Kachkachi, F. Gendron, F. Ott, B. Berini, and N. Keller, Magnetic anisotropies in ultrathin bismuth iron garnet films, J. Magn. Magn. Mater. **335** (2013) 139-143.

[33] S. Geller, J. P. Remeika, R. C. Sherwood, H. J. Williams, and G. P. Espinosa, Magnetic Study of the Heavier Rare-Earth Iron Garnets, Phys. Rev. **137** (1965) A1034.
[34] Y. M. Lu, Y. Choi, C. M. Ortega, X. M. Cheng, J. W. Cai, S. Y. Huang, L. Sun, and C. L. Chien, Pt Magnetic Polarization on $Y_3Fe_5O_{12}$ and Magnetotransport Characteristics, Phys. Rev. Lett. **110** (2013) 147207.
[35] S. Y. Huang, X. Fan, D. Qu, Y. P. Chen, W. G. Wang, J. Wu, T. Y. Chen, J. Q. Xiao, and C. L. Chien, Transport Magnetic Proximity Effects in Platinum, Phys. Rev. Lett. **109** (2012) 107204.
[36] S. Shimizu, K. S. Takahashi, T. Hatano, M. Kawasaki, Y. Tokura, and Y. Iwasa, Electrically Tunable Anomalous Hall Effect in Pt Thin Films, Phys. Rev. Lett. **111** (2013) 216803.
[37] B. F. Miao, S. Y. Huang, D. Qu, and C. L. Chien, Physical Origins of the New Magnetoresistance in Pt/YIG, Phys. Rev. Lett. **112** (2014) 236601.